Manipulation of electronic phases in Au-nanodots-decorated manganite films by laser illumination

Hui Li,[1,2] Kaixuan Zhang,[1,2] Dongli Wang,[1,2] Han Xu,[1,2] Haibiao Zhou,[3,4] Xiaodong Fan,[1,2] Guanghui Cheng,[1,2] Long Cheng,[1,2] Qingyou Lu,[3,4] Lin Li,[1,2,*] and Changgan Zeng[1,2,*]

[1]*International Center for Quantum Design of Functional Materials, Hefei National Laboratory for Physical Sciences at the Microscale, and Synergetic Innovation Center of Quantum Information and Quantum Physics, University of Science and Technology of China, Hefei, Anhui 230026, China*

[2]*CAS Key Laboratory of Strongly Coupled Quantum Matter Physics, and Department of Physics, University of Science and Technology of China, Hefei, Anhui 230026, China*

[3]*High Magnetic Field Laboratory, Chinese Academy of Sciences, Hefei, Anhui 230031, China*

[4]*Collaborative Innovation Center of Advanced Microstructure, Nanjing University, Nanjing, Jiangsu 210093, China*

(Received 20 October 2017; published 6 June 2018)

Precise manipulation of the electronic phases in strongly correlated oxides offers an avenue to control the macroscopic functionalities, thereby sparking enormous research interests in condensed matter physics. In the present paper, phase-separated $La_{0.33}Pr_{0.34}Ca_{0.33}MnO_3$ (LPCMO) thin films with a fraction of the ferromagnetic metallic phase close to the percolation threshold are successfully prepared, in which the nonvolatile and erasable switching between different electronic states is realized through cooperative effects of Au-nanodots capping and laser illumination. The deposition of Au nanodots on LPCMO thin films leads to the occurrence of a thermally inaccessible nonpercolating state at low temperatures, manifested as the absence of insulator-metal transition as temperature decreases. Such a nonpercolating state can be substantially tuned back to a percolating state by laser illumination in a nonvolatile and erasable way, accompanied by gigantic resistance drops in a wide temperature range. The formation of local oxygen vacancies near Au nanodots and thereby the modulation of mesoscopic electronic texture should be the key factor for the realization of flexible modulation of global transport properties in LPCMO thin films. Our findings pave a way toward the manipulation of physical properties of the electronically phase-separated systems and the design of optically controlled electronic devices.

DOI: 10.1103/PhysRevMaterials.2.064403

I. INTRODUCTION

Electronic inhomogeneity, that is, the coexistence of different electronic phases in a structurally homogenous medium, is the key for the emergence of many intriguing properties exhibited in many strongly correlated oxides, including cuprate superconductors and colossal magnetoresistance materials [1–3]. In particular, by manipulating the distribution and evolution of competing electronic phases, novel transport and magnetic properties could be obtained, thus eventually approaching the designed functionalities [4,5]. Doped perovskite manganites, with a hallmark of electronic phase separation, where the antiferromagnetic charge-ordered insulating phase, ferromagnetic metallic (FMM) phase, and paramagnetic insulating phase may coexist at certain situations, have provided an ideal platform to that end [4–10]. The subtle balance between these competing electronic phases at very similar energy scales can be readily broken by various external perturbations, e.g., temperature, strain, magnetic field, and light irradiation [11–21].

Recently, many novel approaches have also been attempted toward the phase manipulation in manganites, for example, by interacting with metal particles [22–25], by direct laser interference illumination [26], and by applying electric field [27,28]. Nevertheless, the realization of the conversion between different electronic states in manganites in a nonvolatile and erasable manner through phase manipulation has not been well demonstrated until now. Here, by a combination of Au-nanodots capping and laser illumination, the mesoscopic electronic texture in $La_{0.33}Pr_{0.34}Ca_{0.33}MnO_3$ (LPCMO) thin films can be tailored without changing the geometries. As a consequence, the global electronic transport properties of the Au-nanodots-capped LPCMO thin films (Au/LPCMO thin films) can be switched easily between percolating and nonpercolating states in a nonvolatile and erasable way.

II. EXPERIMENTAL METHODOLOGY

The LPCMO thin films were grown on the (001)-$LaAlO_3$ (LAO) substrates by pulse laser deposition [29]. For the preparation of the Au/LPCMO samples, Au nanodots with a nominal thickness of 1.5 nm were thermally evaporated onto the LPCMO thin films at a rate of 0.2 nm/s. After that, Au electrodes were sputtered on the thin films for subsequent two-terminal transport measurements. The transport properties of the devices were investigated using a multifunction probe equipped with a standard power single fiber assembly in the Quantum Design physical property measurement system. The wavelength of the adopted cw laser is 532 nm and the light power is 0.9 mW unless otherwise clarified. A specific sample holder with a temperature sensor mounted right under the sample was adopted. The distance between electrodes for all the LPCMO thin films is about 1 mm and the laser spot could fully cover the gap. The magnetic properties were measured in

*Corresponding author: lilin@ustc.edu.cn; cgzeng@ustc.edu.cn

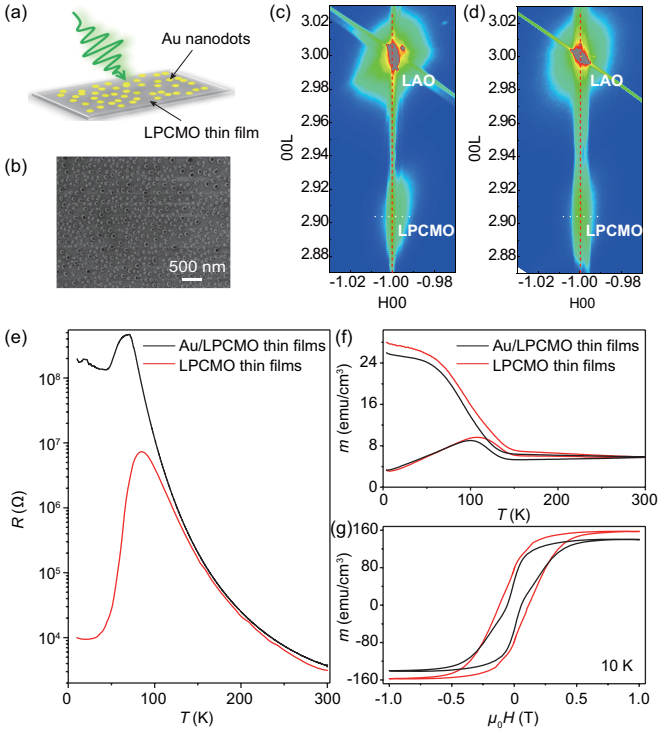

FIG. 1. Effects of Au-nanodots capping on the structural and physical properties of the LPCMO thin films. (a), (b) Schematic drawing and SEM image of the Au/LPCMO thin films, respectively. (c), (d) Reciprocal space maps of the pristine LPCMO thin films and the Au/LPCMO thin films, respectively. The diffraction patterns were presented in the reciprocal units of the $LaAlO_3$ substrate. (e) R-T curves of the pristine LPCMO thin films and the Au/LPCMO thin films obtained at zero magnetic field. (f) Temperature-dependent magnetic moment m of the LPCMO thin films before and after Au-nanodots capping measured after ZFC and FC. (g) Magnetic field-dependent magnetic moment m of the LPCMO thin films before and after Au-nanodots capping measured at 10 K.

the Quantum Design vibrating-sample magnetometer system and superconducting quantum interference device (SQUID) system. The applied magnetic field is 200 Oe for both zero-field cooling (ZFC) and field cooling (FC) measurements. For the measurement of photoinduced magnetization, the magneto-optic probe was adopted in the SQUID system.

III. EXPERIMENTAL RESULTS AND DISCUSSION

Figure 1(a) shows the schematic of the Au/LPCMO thin films; the thickness of the LPCMO film is about 25 nm. As shown in the scanning electron microscopy image in Fig. 1(b), the Au nanodots with an average size and density of about 80 nm and 69/μm^2, respectively, are randomly distributed on the surface of the LPCMO thin films. Figure 1(c) shows the reciprocal space maps for the (103) diffraction peak; the LPCMO thin films and the LAO substrates share the same in-plane lattice value, suggesting that the LPCMO thin films are well epitaxially grown on the LAO substrates and are coherently strained. No noticeable changes are observed after Au-nanodots capping [Fig. 1(d)]. The out-of-plane parameters (lattice constant c) for the LPCMO thin films with and without Au-nanodots capping are estimated to be 3.9107 and 3.9118 Å, respectively, from the x-ray θ-2θ diffraction scans (for details, see Appendix A in the Supplemental Material [30]). Such a tiny deviation of about 0.028% indicates that the deposition of Au nanodots has little influence on the structure of the LPCMO thin films.

Figure 1(e) shows the temperature (T) dependence of the resistance (R) for both the pristine LPCMO thin films and the Au/LPCMO thin films. As the temperature decreases, the pristine LPCMO thin films show a transition from an insulating behavior to a metallic one, with a resistance peak appearing at 83 K. In sharp contrast, the resistance of the Au/LPCMO thin films increases continuously as temperature decreases to about 70 K, and then decreases slightly when the temperature further decreases from 70 to 45 K. Below 45 K, the resistance is almost unchanged. The resistance value of the Au/LPCMO thin films at 10 K is approximately 2×10^8 Ω, which is over four orders of magnitude larger than that of the pristine LPCMO thin films. For typical phase-separated manganites, the significant increasement of the low-temperature resistance normally correlates with the fraction decrease of the FMM phase. To further demonstrate it, the magnetic properties of the same LPCMO thin film before and after Au-nanodots capping were investigated. Figure 1(f) shows the temperature dependence of the magnetic moment m of the pristine LPCMO thin films and the Au/LPCMO thin films measured under 200 Oe after ZFC and FC process. As can be seen, the Curie temperature T_c decreases from ∼149 to ∼138 K after Au-nanodots capping (for the estimation of T_c, see Appendix B in the Supplemental Material [30]). Also, the saturation magnetic moment of the Au/LPCMO thin films at 10 K also gets smaller compared with the pristine LPCMO thin films [see Fig. 1(g)]. The reduction of both the saturation moment and T_c indicates that the suppression of the ferromagnetism induced by Au-nanodots capping. It is noted that the fraction of the FMM phase at low temperatures in Au/LPCMO thin films should be just slightly lower than the threshold for the emergence of percolation transport, as the resistance changes very little when the temperature decreases below 45 K [see Fig. 1(e)], exhibiting tunneling-like behavior instead of exponentially increasing tendency generally seen in typical insulators [31,32]. Thus, the shrunken insulating domains may act as intrinsic tunneling barriers to allow electrons tunneling between its two neighboring FMM domains, even though the well-defined conducting paths are not formed through connecting FMM domains.

In Appendix C in the Supplemental Material [30], the possible mechanisms which may account for the suppression of the ferromagnetism and conductivity of the Au/LPCMO thin films are carefully checked, and the formation of oxygen vacancies in the LPCMO thin films should be the most reasonable mechanism. Distinct from Au bulk, Au nanodots with small size possess high reactivity [33]. The deposited Au nanodots could extract oxygen from the LPCMO thin films, and induce local oxygen vacancies in the proximal LPCMO films. Such oxygen vacancies will render the double-exchange interaction weaker, and thus lead to the fraction decrease of the FMM phase [22,23]. Nevertheless, the amount of the oxygen vacancies should be little, as the change of lattice structure after Au-nanodots capping is negligible [see Figs. 1(c) and 1(d)].

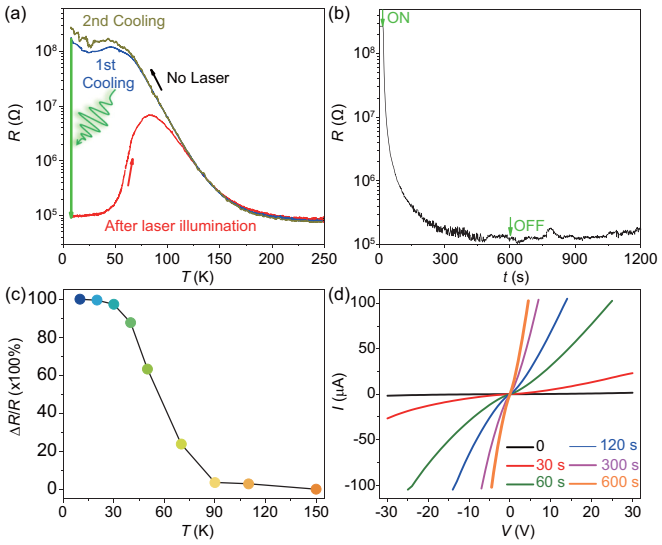

FIG. 2. Photoinduced resistance drops in the Au/LPCMO thin films. (a) R-T curves of the Au/LPCMO thin films before (blue curve) and after (red curve) laser illumination. The yellow curve is the R-T curve of the Au/LPCMO thin films obtained in the recooling process. (b) R as a function of time for the Au/LPCMO thin films under laser illumination at 10 K. (c) The magnitude of photoinduced resistance drop, defined as $\Delta R = \frac{R(0)-R(600s)}{R(0)} \times 100\%$, as a function of temperature for the Au/LPCMO thins films. (d) I-V curves of the Au/LPCMO thin films measured in the dark after laser illumination for different durations at 10 K.

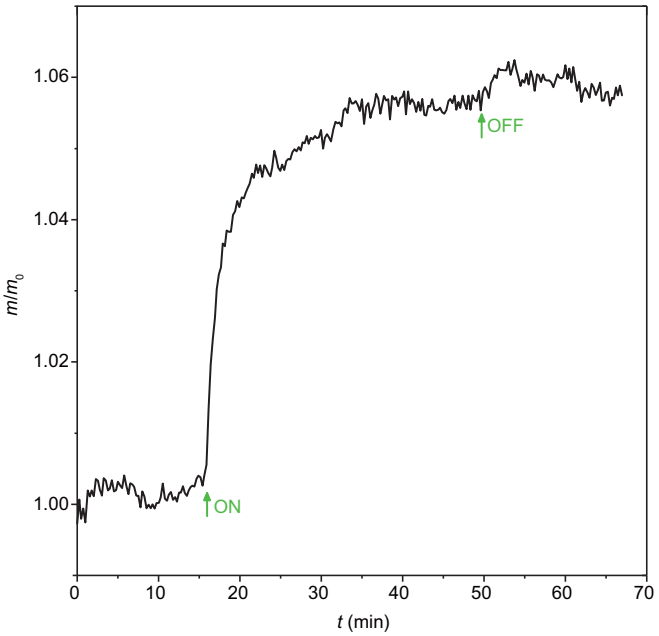

FIG. 3. Photoinduced enhancement of magnetic moment of the Au/LPCMO thin films, in which m_0 and m denote the magnetic moment of Au/LPCMO thin films at time zero and time t, respectively.

Next we will demonstrate the nonvolatile and erasable modulation of electronic states in the Au/LPCMO thin films realized via laser illumination. As indicated by the blue curve in Fig. 2(a), the resistance of the Au/LPCMO thin films stabilizes at around $10^8\ \Omega$ below 45 K when cooling down from room temperature in the dark. Once the cw laser is switched on at 10 K, the resistance drops dramatically to $\sim 10^5\ \Omega$. The positive slope of the measured R-T curve during the subsequent warming process with the laser switched off (see the red curve) indicates that the Au/LPCMO thin films are metallic at low temperatures after laser illumination. The Au/LPCMO thin films undergo a metal-insulator transition at about 90 K in the warming process, which is similar to the R-T curve of pristine LPCMO thin films [Fig. 1(e)]. The photoinduced insulator-metal transition (IMT) demonstrates that the fraction of the FMM phase in the Au/LPCMO thin films gets above the percolation threshold after laser illumination, and a global percolating state is eventually obtained. It should be noted that such photoinduced transition from the nonpercolating state to the percolating state is erasable, as the nonpercolating state is reproducible by cooling the Au/LPCMO thin films in the dark from high temperature again. As shown in the dark yellow curve in Fig. 2(a), the R-T curve measured in the second cooling process is nearly the same as the one obtained in the first cooling process.

To better illustrate the dynamics of photoinduced resistance drops, the resistance of the Au/LPCMO thin films as a function of illumination time was measured. As can be seen in Fig. 2(b), the resistance quickly drops initially after irradiation by laser, and finally reaches $\sim 10^5\ \Omega$ in 450 s at 10 K. The resistance value persists even after the laser is switched off at 600 s, behaving as a nonvolatile characteristic. This feature rules out the possibility of laser induced local heating effects on the photoinduced resistance drops in the Au/LPCMO thin films. Moreover, similar nonvolatile photoinduced resistance drops can be obtained in a wide temperature range (for details, see Appendix D in the Supplemental Material [30]). As shown in Fig. 2(c), the magnitude of resistance drop, defined as $\Delta R = \frac{R(0)-R(600s)}{R(0)} \times 100\%$, decays gradually with increasing temperature, and eventually disappears at $\sim$150 K, which is close to the T_c of the pristine LPCMO thin films ($\sim$149 K) shown in Fig. 1(f). Furthermore, the nonvolatility also enables us to conduct the current (I) versus voltage (V) measurements in the dark after laser illumination for different durations, from which the photoinduced emergence of the metallic state is also evidenced. As shown in Fig. 2(d), when the illumination time increases, the I-V curve changes from a nonlinear to an approximately linear character.

As the magnetic properties and the electronic transport properties of manganites are strongly coupled, the magnetic properties of the Au/LPCMO thin films before and after laser illumination were also investigated. Figure 3 shows the evolution of magnetic moment under laser illumination obtained at 10 K and 0.1-T magnetic field applied perpendicular to the Au/LPCMO thin-film plane. When the laser is switched on, the magnetic moment increases sharply at the start and then gradually saturates. The magnetic moment persists even after the laser is switched off. Consisting with the increase of the conductivity (Fig. 2), the enhancement of the magnetic moment further demonstrates the fraction increase of the FMM phase under laser illumination. Nevertheless, the magnitude of the magnetic moment for the whole Au/LPCMO thin film only

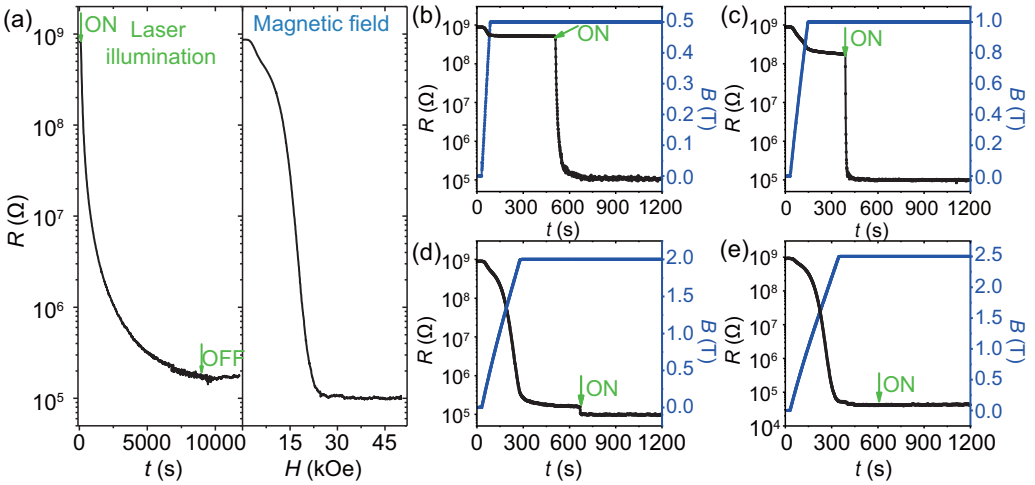

FIG. 4. Synergistic effects of laser illumination and magnetic field on the electronic transport properties of Au/LPCMO thin films at 10 K. (a) Comparison of the photoinduced (left panel) and magnetic field induced (right panel) resistance drops. (b)–(e) Photoinduced resistance drops under different magnetic fields. When the applied magnetic field is smaller than 2.25 T, the laser illumination would further trigger resistance drops (b)–(d), while no photoinduced resistance drops can be observed when the magnetic field further increases to 2.5 T (e).

increases by about 6% after laser illumination, indicating the fraction increase of the FMM phase is relatively small.

For typical phase-separated manganites like LPCMO, gigantic resistance drops can also be obtained via applying magnetic field at low temperatures. To compare the effects of these two different external fields, the synergistic effects of laser illumination and magnetic field on the electronic transport properties of the Au/LPCMO thin films were measured, as shown in Fig. 4. The value of resistance drop induced by laser illumination is roughly equivalent to the effect by applying 2.25-T magnetic field [Fig. 4(a)]. Figures 4(b)–4(e) show the photoinduced resistance drops measured at different magnetic fields. When the magnetic field is smaller than 2.25 T, the laser illumination would further trigger resistance drop [Figs. 4(b)–4(d)], while no photoinduced resistance drops can be observed when the magnetic field is increased above 2.25 T [Fig. 4(e)]. Such synergistic characteristics indicate that the photoinduced resistance drops in the Au/LPCMO thin films is phenomenologically the same as magnetic field effects, arising from the fraction increase of the FMM phase at the expense of insulating phases. However, the mesoscopic mechanisms differ essentially. The magnetic field would effectively align the spins of the Mn ions, favoring the hopping of the electrons between the Mn ions via the double-exchange interaction. While the laser illumination would generate electron-hole pairs. The electrons are trapped at the oxygen vacancies while the holes contribute to the enhanced conductivity, as demonstrated later.

The laser illumination effect on the pristine LPCMO thin films with similar thickness was also measured for comparison, in which negligible resistance drop was obtained. Therefore, the significant enhancement of photosusceptibility of the Au/LPCMO thin films should be mainly attributed to the occurrence of oxygen vacancies induced by Au-nanodots capping. In Appendix E in the Supplemental Material [30], the possible mechanisms for the photoinduced resistance drops in the Au/LPCMO thin films have been discussed in detail. To better clarify the mechanism, a simplified schematic drawing for the evolution of electronic phases induced by the cooperative effects of Au-nanodots capping and laser illumination is summarized in Figs. 5(a)–5(c). It is well known that percolation transport is the key mechanism for the low-temperature

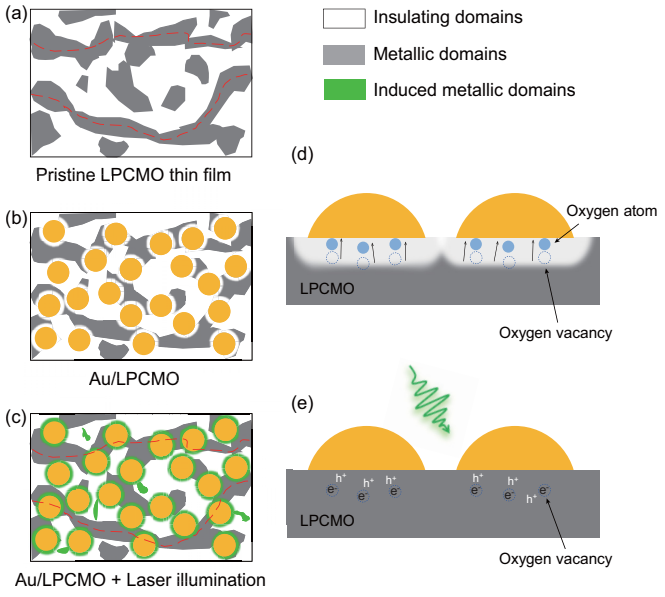

FIG. 5. Schematic drawing for the manipulation of electronic phases in the LPCMO thin films with Au-nanodots capping and under laser illumination. (a) Coexistence of metallic and insulating phases in the pristine LPCMO thin films. The conducting paths (dashed red curves) are formed through connecting metallic domains. (b), (d) Local extraction of oxygen from LPCMO thin films by Au nanodots results in the formation of local insulating domains, leading to the blocking of the conducting paths and the occurrence of the nonpercolating state at low temperatures. (c), (e) The laser illumination induces the formation of electron-hole pairs, where electrons are trapped by oxygen vacancies and holes participate in the conduction process. The newly induced metallic domains lead to the formation of new conducting paths (dashed red curves), and the percolating state is finally reentered at low temperatures.

electronic transport of electronically phase-separated manganites [32]. For LPCMO, as temperature decreases, the fraction of the FMM phase increases continuously at the expense of the insulating phases. When the fraction of the FMM phase is above the percolation threshold at low temperatures, e.g., in our pristine LPCMO thin films with the thickness of 25 nm, conducting paths are formed through the connected FMM domains [as shown in the dashed red lines in Fig. 5(a)]. A percolating state with low residual resistance at low temperatures is thus obtained [see the red curve in Fig. 1(e)]. When Au nanodots are deposited, local insulating domains are induced in the proximal LPCMO thin films. According to the relative high distribution density of Au nanodots on the surface of the LPCMO thin films, the top affected part of the LPCMO thin films will become insulating due to the fraction decrease of the FMM phase. Also, as the percolation threshold of manganites thin films increases with decreasing thickness (as discussed later), the bottom unaffected part [the gray areas in Fig. 5(d)] could also become nonpercolating due to the increasing percolation threshold compared with the pristine LPCMO thin films even the fraction of the FMM phase remains unchanged. As a result, an overall nonpercolating state with high residual resistance is observed in the Au/LPCMO thin films [black curve in Fig. 1(e)]. When the laser is switched on, newly induced FMM domains emerge mainly around Au nanodots [as indicated by the green areas in Fig. 5(c)], which makes the fraction of the FMM phase over the percolation threshold. The conducting paths are developed again [see the dashed red lines in Fig. 5(c)], leading to the occurrence of gigantic resistance drops at low temperatures. The emergence of the photoinduced FMM domains can be explained as follows: the incident photons generate electron-hole pairs in the LPCMO thin films. The electrons are easily trapped at the oxygen vacancies while the holes contribute to the conduction process [Fig. 5(e)] [34–37]. Since the electrons are trapped at the oxygen vacancies, the recombination of electrons and holes is suppressed, which thus results in the nonvolatile resistance drops after the laser is switched off. By heating the samples to high temperature, the electrons gain enough energy to escape from the oxygen vacancies to recombine with the holes, and eventually erase the photoconductivity effect.

Here, we would like to emphasize that the success of the electronic state manipulation relies on preparing LPCMO thin films with the fraction of the FMM phase close to the percolating and nonpercolating boundary, which enables the system to cross the boundary back and forth readily by adopting multiple external perturbations, and therefore exhibiting intriguing modulations of the global transport properties. Such requirement was realized via precisely controlling the thickness of LPCMO thin films in our experiments. For a typical phase-separated system, the value of the percolation threshold for the emergence of the percolating state depends strongly on the dimensionality of the system, e.g., about 25 and 50% for a three-dimensional simple cubic lattice and two-dimensional square lattice, respectively [38]. For the LPCMO system with the chemical stochiometry adopted in the present paper, the percolation threshold should be far below the fraction of the FMM phase at low temperatures in the bulk or thick films, as evidenced from the metallic behavior at low temperatures. When the film thickness is reduced, the percolation threshold is expected to increase accordingly, from the typical three-dimensional value to the two-dimensional value. Therefore, it is possible to adjust the percolation threshold to get close to the fraction of the FMM phase in LPCMO thin film via simply reducing the film thickness.

To further demonstrate this point, the effects of Au-nanodots capping were studied on two LPCMO thin-film samples with different thicknesses of ∼30 nm (sample S1) and ∼40 nm (sample S2) for comparison, as shown in Appendix F in the Supplemental Material [30]. Sample S1 can be easily converted to the nonpercolating state at low temperatures when the Au nanodots were deposited. In contrast, sample S2 still shows metallic behavior at low temperatures, and the Au-nanodots capping only reduces the IMT temperature. These observations strongly support the picture that the percolation threshold can be tuned by controlling the film thickness, which enables the effective manipulation of the transport properties for the Au-nanodots-decorated LPCMO films via light illumination.

The nonvolatile photoinduced gigantic resistance drops have also been observed in low La doping (La,Pr,Ca)MnO_3 thin films [18,39,40]. It is emphasized here that the manipulation manner of electronic phases in our paper differs substantially from the previous studies, in which the modulations are usually homogeneous in nature. In sharp contrast, the present paper utilizes local modulation of the electronic phases in manganite thin films. The local insulating domains that are not energetically favorable are obtained at low temperatures in the proximity of Au nanodots. Most of these insulating domains will be converted into metallic under subsequent laser illumination, and thus play a major role in the global transition from nonpercolating state to percolating state. In addition, if the Au nanodots are further spatially patterned on the LPCMO thin films, e.g., forming periodic strip arrays, the periodic nonpercolating and percolating patterns in a structurally uniform medium can be conveniently achieved. Such a route for tailoring electronic phases, which can be regarded as a prototype of so-called electronic fabrication [41,42], will have promising application toward functionalities explorations.

IV. CONCLUSION

In conclusion, cooperative effects of Au-nanodots capping and laser illumination on the transport properties of LPCMO thin films have been exploited. The local insulating domains are induced due to the extraction of oxygen from LPCMO thin films by Au nanodots, leading to a nonpercolating state at low temperatures. When the laser illumination is subsequently switched on, the nonpercolating state can be switched back to a percolating state in a nonvolatile way. Moreover, such a photoinduced percolating state can be easily erased by thermal cycling. Our findings would further promote the realization of engineering desired patterns of competing phases in manganites. Such a route for the manipulation of electronic phases will underpin the understanding of the coexistence and competition between various electronic phases, and further inspire functional applications.

ACKNOWLEDGMENTS

This paper was supported by the National Basic Research Program of China (Grant No. 2014CB921102), National

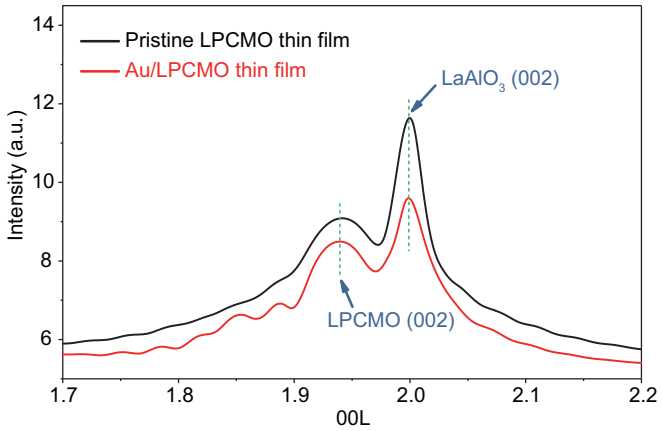

FIG. 6. X-ray θ-2θ diffraction scans of the (002) peak for 25-nm LPCMO/LAO thin films with (red curve) and without (black curve) Au-nanodots capping.

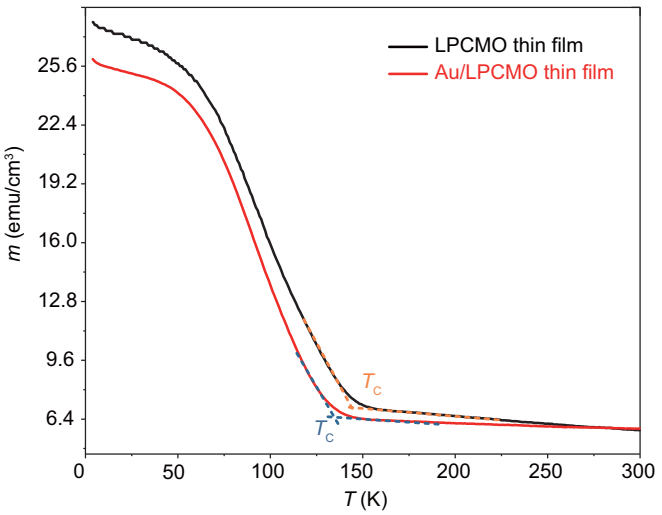

FIG. 7. Definition of T_c from the m-T curves.

Key Research and Development Program of China (Grants No. 2017YFA0403600 and No. 2017YFA0402903), National Natural Science Foundation of China (Grants No. 11434009 and No. 11461161009), Fundamental Research Funds for the Central Universities (Grant No. WK2030020027), National Natural Science Foundation of China/Research Grants Council of Hong Kong Joint Research Scheme (Grant No. N-PolyU517/14), and Anhui Provincial Natural Science Foundation (Grant No. 1708085QA20).

H.L. and K.Z. contributed equally to this paper.

APPENDIX A: X-RAY θ-2θ DIFFRACTION PATTERNS FOR LPCMO THIN FILMS AND AU/LPCMO THIN FILMS

X-ray θ-2θ diffraction scans were performed to study the crystalline quality and lattice parameters of the films, and the results are shown in Fig. 6. The out-of-plane parameters (lattice constant c) for the LPCMO thin films with and without Au-nanodots capping are estimated to be 3.9107 and 3.9118 Å, respectively. Such a tiny deviation of about 0.028% indicates that the deposition of Au nanodots has little influence on the structure of the LPCMO thin films.

APPENDIX B: THE CURIE TEMPERATURE T_c FOR THE m-T CURVES

The T_c is defined as the temperature corresponding to the intersection of the linear fitting curves at the transition region, as shown in Fig. 7 below. The T_c for the pristine LPCMO thin films and the Au/LPCMO thin films is estimated to be ∼149 and ∼138 K, respectively.

APPENDIX C: MECHANISMS FOR THE MODIFICATION OF PHYSICAL PROPERTIES OF LPCMO THIN FILMS AFTER AU-NANODOTS CAPPING

As illustrated in the main text, Au-nanodots capping leads to the suppression of the ferromagnetism and conductivity of the LPCMO thin films, suggesting the fraction decrease of the FMM phase in the LPCMO thin films. Here we discuss the possible mechanisms which may account for this effect.

1. Electrostatic effect

When metal nanodots are deposited on the surface of manganites, charge transfer may happen due to the misalignment of their work functions. In our experiment, the work functions of Au and LPCMO are 5.1 and 4.9 eV, respectively. Therefore, a net electron transfer from LPCMO to Au is expected, which will increase the hole concentration in the LPCMO thin films and thus lead to the enhancement of ferromagnetism and conductivity. Such expectations, however, are opposite to our experimental findings shown in Figs. 1(e)–1(g), where the ferromagnetism and conductivity are both suppressed.

2. Formation of oxygen vacancies

Distinct from Au bulk, Au nanodots with small size possess high reactivity [33]. The deposited Au nanodots could extract oxygen from the LPCMO thin films, and induce local oxygen vacancies in the proximal LPCMO films. Such oxygen vacancies will render the double-exchange interaction weaker, and thus lead to the fraction decrease of the FMM phase [22,23]. In fact, the formation of oxygen vacancies has been revealed experimentally in a previous study of Au/$La_{0.67}Sr_{0.33}MnO_3$, and was proposed to be the main cause to drive the observed huge decrease of the conductivity and Curie temperature of the $La_{0.67}Sr_{0.33}MnO_3$ films [23]. Furthermore, suppression of ferromagnetism and conductivity has been generally observed for manganites with oxygen vacancies [35,43–46].

Based on the above discussion, formation of oxygen vacancies should be the most reasonable mechanism accounting for the suppression of the ferromagnetism and conductivity of the LPCMO thin films after Au-nanodots capping. Moreover, this mechanism is also consistent with the observed photoinduced resistance drops, as detailed in the main text and Appendix E.

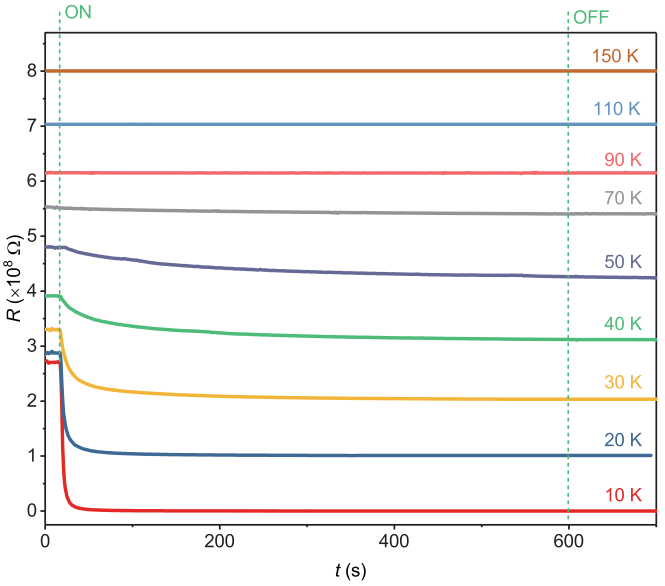

FIG. 8. Photoinduced resistance drops of the Au/LPCMO thin films at different temperatures.

APPENDIX D: TEMPERATURE DEPENDENCE OF THE PHOTOINDUCED RESISTANCE DROPS IN AU/LPCMO THIN FILMS

The photoinduced resistance drops in Au/LPCMO thin films are shown in Fig. 8.

APPENDIX E: POSSIBLE MECHANISM OF PHOTOINDUCED EFFECTS IN AU/LPCMO THIN FILMS

For the Au/LPCMO thin films, laser illumination could induce a nonvolatile and erasable transition from nonpercolating state to percolating state, accompanied by gigantic resistance drops at low temperatures. We discuss the possible mechanisms as follows.

First, the plasmon effect can be excluded to cause the gigantic resistance drops.

Figure 9(a) shows the optical absorption spectra of the same piece of LPCMO thin film before and after Au-nanodots capping. Compared with the pristine LPCMO thin films, an obvious absorption peak at around 555 nm emerges after Au-nanodots capping, corresponding to the plasmon resonance absorption of the Au nanodots [47]. In a controlled experiment, lasers with wavelengths of 404 and 532 nm were adopted. Because the plasmon resonance absorption is around 555 nm, plasmon excitation can only be launched by the 532-nm laser illumination. As shown in Fig. 9(b), no significant difference can be observed from the time-dependent resistance curves under the illumination of the 404- and 532-nm lasers with the same power. These observations clearly demonstrate that the plasmon effect of Au nanodots cannot account for the photoinduced resistance drops in the Au/LPCMO thin films.

Secondly, similar photoinduced resistance drops with nonvolatile characteristics have been widely observed in oxygen-deficient manganite [35,36,48] and cuprate [34] systems. It has been well established that in such oxygen-deficient systems the light illumination generates electron-hole pairs.

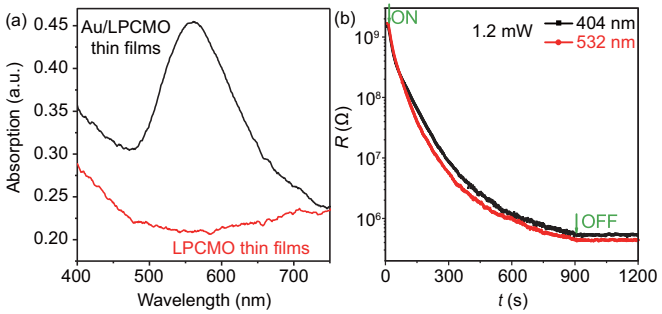

FIG. 9. Exclusion of the plasmon effect on the photoinduced resistance drops in the Au/LPCMO thin films. (a) Absorption spectra of the pristine LPCMO thin films and the Au/LPCMO thin films. (b) Resistance of the Au/LPCMO thin films as a function of time under laser illumination with different wavelengths and the same power at 10 K.

The electrons are trapped at the oxygen vacancies while the holes contribute to the enhanced conductivity. By heating the samples to high temperature, the electrons gain enough energy to escape from the oxygen vacancies to recombine with the holes, and eventually erase the photoconductivity effect. Such mechanism can naturally explain the observed photoinduced gigantic resistance drops in the Au/LPCMO thin films with oxygen vacancies in the LPCMO part.

Moreover, as demonstrated below, the transport results of the Au/LPCMO thin films can be well understood from this mechanism.

1. Temperature dependence of the nonvolatile photoinduced resistance drops in the Au/LPCMO thin films

As shown in Fig. 2(c) in the main text, the nonvolatile photoinduced resistance drops in the Au/LPCMO thin films decays gradually with increasing temperature, and eventually disappears at ∼150 K, which is close to the T_c of the pristine LPCMO thin films (∼149 K). This characteristic could be explained by the decrease of both the fraction of intrinsic FMM phase and the amount of photoinduced FMM phase in the Au/LPCMO thin films with increasing temperature. The former issue has been widely observed in previous studies of the phase-separated manganites [5,20], while the amount of decrease of the photoinduced FMM phase with increasing temperature is probably related to the increased recombination rate of the photogenerated electrons and the holes.

As illustrated above, the oxygen vacancies could trap the photogenerated electrons while the holes contribute to the increased conductivity and fraction of the FMM phase in the Au/LPCMO thin films. At low temperatures, the trapped electrons cannot escape from the oxygen vacancies to recombine with the holes, due to their relatively small kinetic energy compared to the potential barrier of the oxygen vacancies. As the temperature increases, the kinetic energy of the trapped electrons increases, leading to the increase of recombination rate of the trapped electrons and the holes. As a result, the amount of photoinduced FMM phase decreases accordingly.

When the temperature increases further, e.g., above T_c of the pristine LPCMO thin films, no FMM phase exists in the LPCMO thin films, and the amount of photoinduced FMM

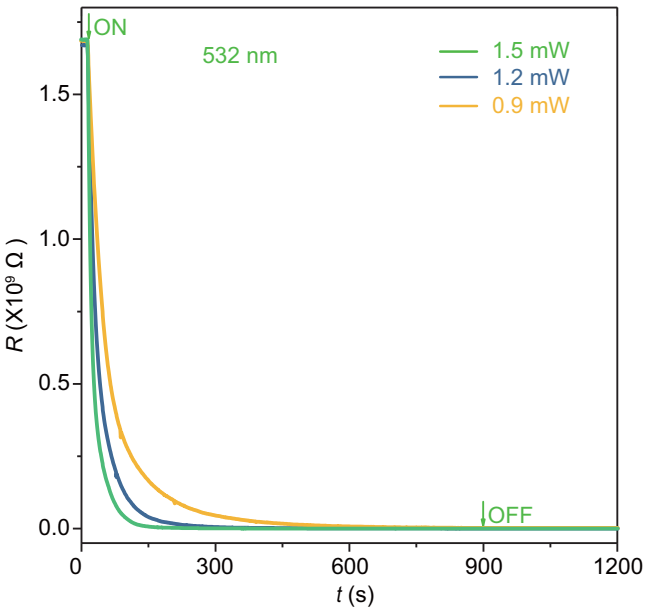

FIG. 10. Resistance of the Au/LPCMO thin films as a function of time under laser illumination with different powers at 10 K. A laser wavelength of 532 nm is adopted.

phase is also negligible, thus the photoinduced resistance drops vanish eventually.

2. Relatively long characteristic time of the photoinduced resistance drops in the Au/LPCMO thin films

As shown in Fig. 2(b) in the main text, it takes hundreds of seconds for the resistance to reach a stable low value under light illumination. Such a long characteristic time can be attributed to the time-consuming electrons trapping processes at the oxygen vacancies and the relatively long spin-lattice relaxation time due to the phase-separated character of LPCMO. As illustrated in Appendix C, the local oxygen vacancies are induced in the proximity of Au nanodots in the Au/LPCMO thin films due to the high reactivity of the Au nanodots. These oxygen vacancies serve as the trapping sites to trap the photogenerated electrons, and the photogenerated holes contribute to the enhanced conductivity. Therefore, the photoconductivity in such system increases with increasingly cumulative photon dose,

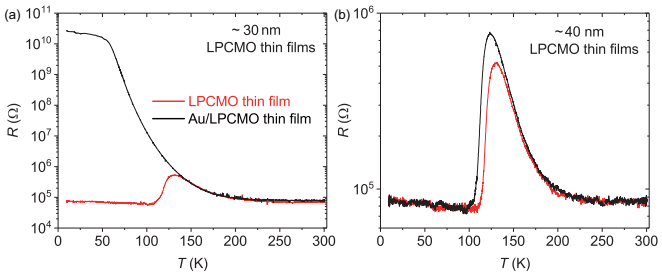

FIG. 11. *R-T* curves of the LPCMO thin films with different thicknesses of ∼30 nm (a) and ∼40 nm (b) before and after Au-nanodots capping, respectively.

and saturates gradually as the illumination time increases. On the other hand, LPCMO is a typical phase-separated material with the coexistence of metallic and insulating domains. The interface strain due to their slight lattice mismatch [19] prevents the spin-lattice relaxation process, and eventually increases the relaxation time, which has been revealed previously in the manganites [18,39].

3. Laser power dependence of the photoinduced resistance drops in the Au/LPCMO thin films

The resistance (R) of the Au/LPCMO thin films as a function of illumination time at different laser powers is shown in Fig. 10. When the laser power increases from 0.9 to 1.5 mW, the characteristic time reduces from ∼450 to ∼150 s. Since the photoinduced resistance drops in the Au/LPCMO is related to the electrons trapping process at the oxygen vacancies, it will become saturated when the number of incident photons reaches a certain value. When the laser power increases, the incident photon flux increases accordingly, resulting in a shorter characteristic time.

APPENDIX F: THE TRANSPORT PROPERTIES OF AU-NANODOTS-DECORATED LPCMO THIN FILMS WITH DIFFERENT THICKNESSES

R-T curves of the LPCMO thin films with different thicknesses before and after Au-nanodots capping are shown in Fig. 11.

[1] E. Dagotto, T. Hotta, and A. Moreo, Phys. Rep. **344**, 1 (2001).
[2] E. Dagotto, Science **309**, 257 (2005).
[3] B. Chen, H. Xu, C. Ma, S. Mattauch, D. Lan, F. Jin, Z. Guo, S. Wan, P. Chen, G. Gao, F. Chen, Y. Su, and W. Wu, Science **357**, 191 (2017).
[4] M. Fäth, S. Freisem, A. A. Menovsky, Y. Tomioka, J. Aarts, and J. A. Mydosh, Science **285**, 1540 (1999).
[5] M. Uehara, S. Mori, C. H. Chen, and S. W. Cheong, Nature (London) **399**, 560 (1999).
[6] L. Zhang, C. Israel, A. Biswas, R. L. Greene, and A. de Lozanne, Science **298**, 805 (2002).
[7] W. Wu, C. Israel, N. Hur, S. Park, S.-W. Cheong, and A. de Lozanne, Nat. Mater. **5**, 881 (2006).
[8] A. D. K. Finck, D. J. Van Harlingen, P. K. Mohseni, K. Jung, and X. Li, Phys. Rev. Lett. **110**, 126406 (2013).
[9] K. Lai, M. Nakamura, W. Kundhikanjana, M. Kawasaki, Y. Tokura, M. A. Kelly, and Z.-X. Shen, Science **329**, 190 (2010).
[10] C. Renner, G. Aeppli, B. G. Kim, Y. A. Soh, and S.-W. Cheong, Nature (London) **416**, 518 (2002).
[11] Y. Tomioka, A. Asamitsu, Y. Moritomo, H. Kuwahara, and Y. Tokura, Phys. Rev. Lett. **74**, 5108 (1995).
[12] V. Kiryukhin, D. Casa, J. P. Hill, B. Keimer, A. Vigliante, Y. Tomioka, and Y. Tokura, Nature (London) **386**, 813 (1997).
[13] K. Miyano, T. Tanaka, Y. Tomioka, and Y. Tokura, Phys. Rev. Lett. **78**, 4257 (1997).

[14] K. H. Ahn, T. Lookman, and A. R. Bishop, Nature (London) **428**, 401 (2004).
[15] T. Dhakal, J. Tosado, and A. Biswas, Phys. Rev. B **75**, 092404 (2007).
[16] T. Z. Ward, J. D. Budai, Z. Gai, J. Z. Tischler, L. Yin, and J. Shen, Nat. Phys. **5**, 885 (2009).
[17] M. Rini, R. Tobey, N. Dean, J. Itatani, Y. Tomioka, Y. Tokura, R. W. Schoenlein, and A. Cavalleri, Nature (London) **449**, 72 (2007).
[18] S. Chaudhuri and R. C. Budhani, Europhys. Lett. **81**, 17002 (2007).
[19] S. Majumdar, H. Huhtinen, M. Svedberg, P. Paturi, S. Granroth, and K. Kooser, J. Phys.: Condens. Matter **23**, 466002 (2011).
[20] R. Rawat, P. Kushwaha, D. K. Mishra, and V. G. Sathe, Phys. Rev. B **87**, 064412 (2013).
[21] J. Lourembam, J. Ding, A. Bera, W. Lin, and T. Wu, Appl. Phys. Lett. **104**, 133508 (2014).
[22] R. Bertacco, S. Brivio, M. Cantoni, A. Cattoni, D. Petti, M. Finazzia, and F. Ciccacci, Appl. Phys. Lett. **91**, 102506 (2007).
[23] S. Brivio, C. Magen, A. A. Sidorenko, D. Petti, M. Cantoni, M. Finazzi, F. Ciccacci, R. De Renzi, M. Varela, S. Picozzi, and R. Bertacco, Phys. Rev. B **81**, 094410 (2010).
[24] R. Ferragut, A. Dupaquier, S. Brivio, R. Bertacco, and W. Egger, J. Appl. Phys. **110**, 053511 (2011).
[25] T. Z. Ward, Z. Gai, X. Y. Xu, H. W. Guo, L. F. Yin, and J. Shen, Phys. Rev. Lett. **106**, 157207 (2011).
[26] J. Ding, Z. Lin, J. Wu, Z. Dong, and T. Wu, Small **11**, 576 (2015).
[27] T. Wu, S. B. Ogale, J. E. Garrison, B. Nagaraj, Amlan Biswas, Z. Chen, R. L. Greene, R. Ramesh, T. Venkatesan, and A. J. Millis, Phys. Rev. Lett. **86**, 5998 (2001).
[28] J. Lourembam, J. Wu, J. Ding, W. Lin, and T. Wu, Phys. Rev. B **89**, 014425 (2014).
[29] H. Li, L. Li, L. Li, H. Liang, L. Cheng, X. Zhai, and C. Zeng, Appl. Phys. Lett. **104**, 082414 (2014).
[30] See Supplemental Material at http://link.aps.org/supplemental/10.1103/PhysRevMaterials.2.064403 for XRD patterns of the LPCMO thin film and the Au/LPCMO thin film, temperature, and laser power dependence of photoinduced resistance drop in Au/LPCMO thin films, transport properties of Au-nanodots-decorated LPCMO thin films with different thicknesses, and discussions on the physical mechanism, which includes Refs. [5,18–20,22,23,33–36,39,43–48].
[31] G. Singh-Bhalla, S. Selcuk, T. Dhakal, A. Biswas, and A. F. Hebard, Phys. Rev. Lett. **102**, 077205 (2009).
[32] K. Zhang, L. Li, H. Li, Q. Feng, N. Zhang, L. Cheng, X. Fan, Y. Hou, Q. Lu, Z. Zhang, and C. Zeng, Nano Lett. **17**, 1461 (2017).
[33] D. C. Lim, I. Lopez-Salido, R. Dietsche, M. Bubek, and Y. D. Kim, Chem. Phys. **330**, 441 (2006).
[34] V. I. Kudinov, I. L. Chaplygin, A. I. Kirilyuk, N. M. Kreines, R. Laiho, E. Lahderanta, and C. Ayache, Phys. Rev. B **47**, 9017 (1993).
[35] R. Cauro, A. Gilabert, J. P. Contour, R. Lyonnet, M.-G. Medici, J.-C. Grenet, C. Leighton, and I. K. Schuller, Phys. Rev. B **63**, 174423 (2001).
[36] Z. G. Sheng, Y. P. Sun, J. M. Dai, X. B. Zhu, and W. H. Song, Appl. Phys. Lett. **89**, 082503 (2006).
[37] E. Beyreuther, A. Thiessen, S. Grafstrom, L. M. Eng, M. C. Dekker, and K. Dorr, Phys. Rev. B **80**, 075106 (2009).
[38] S. Kirkpatrick, Rev. Mod. Phys. **45**, 574 (1973).
[39] S. Chaudhuri, N. K. Pandey, S. Saini, and R. C. Budhani, J. Phys.: Condens. Matter **22**, 275502 (2010).
[40] H. J. Lee, K. H. Kim, M. W. Kim, T. W. Noh, B. G. Kim, T. Y. Koo, S.-W. Cheong, Y. J. Wang, and X. Wei, Phys. Rev. B **65**, 115118 (2002).
[41] N. Mathur and P. Littlewood, Nat. Mater. **3**, 207 (2004).
[42] J. Qi, H. Zhang, D. Ji, X. Fan, L. Cheng, H. Liang, H. Li, C. Zeng, and Z. Zheng, Adv. Mater. **26**, 3735 (2014).
[43] J. F. Mitchell, D. N. Argyriou, C. D. Potter, D. G. Hinks, J. D. Jorgensen, and S. D. Bader, Phys. Rev. B **54**, 6172 (1996).
[44] A. M. De Leon-Guevara, P. Berthet, J. Berthon, F. Millot, A. Revcolevschi, A. Anane, C. Dupas, K. Le Dang, J. P. Renard, and P. Veillet, Phys. Rev. B **56**, 6031 (1997).
[45] R. Shiozaki, K. Takenaka, Y. Sawaki, and S. Sugai, Phys. Rev. B **63**, 184419 (2001).
[46] C. Adamo, C. A. Perroni, V. Cataudella, G. De Filippis, P. Orgiani, and L. Maritato, Phys. Rev. B **79**, 045125 (2009).
[47] S. Link and M. A. El-Sayed, J. Phys. Chem. B **103**, 4212 (1999).
[48] G. J. Yong, R. M. Kolagani, B. P. Hofmann, S. Adhikari, Y. Liang, and V. N. Smolyaninova, J. Appl. Phys. **106**, 043902 (2009).